Geochemistry Geophysics Geosystems G3

Article
Volume 13, Number 1
10 February 2012
Q02004, doi:10.1029/2011GC003923
ISSN: 1525-2027

Published by AGU and the Geochemical Society

Shallow lithospheric contribution to mantle plumes revealed by integrating seismic and geochemical data

Jasper G. Konter
Department of Geological Sciences, University of Texas at El Paso, El Paso, Texas 79968, USA (jgkonter@utep.edu)

Thorsten W. Becker
Department of Earth Sciences, University of Southern California, Los Angeles, California 90089, USA

[1] Using an integrated geophysical and geological approach based on a comparative analysis of 27 different parameters, we investigate both the location and origin of the source material for hot spot volcanoes. We report a significant correlation between extreme geochemical compositions of lavas with both shallow seismic velocities and the depth extent to which a hot spot source can be traced with seismic tomography. These relationships provide the first integrated evidence for buoyantly rising plumes of mantle material (plume depth extent correlation), incorporating thermally eroded continental material in the shallow mantle (anti-correlation with slow shallow seismic velocities). The extreme geochemical composition of the lavas is successfully modeled with this process, placing constraints on dynamical processes in the mantle and explaining the origin of a significantly debated mantle compositional end-member (enriched mantle; EM1).

Components: 9200 words, 7 figures, 1 table.

Keywords: EM1; hot spot; mantle components; plume; radiogenic isotopes; seismic velocities.

Index Terms: 1009 Geochemistry: Geochemical modeling (3610, 8410); 1038 Geochemistry: Mantle processes (3621); 7270 Seismology: Tomography (6982, 8180).

Received 17 October 2011; **Revised** 4 January 2012; **Accepted** 5 January 2012; **Published** 10 February 2012.

Konter, J. G., and T. W. Becker (2012), Shallow lithospheric contribution to mantle plumes revealed by integrating seismic and geochemical data, *Geochem. Geophys. Geosyst.*, *13*, Q02004, doi:10.1029/2011GC003923.

1. Introduction

[2] Observations at hot spot volcanoes play an essential role in the unraveling of Earth's thermochemical structure and dynamics. This fundamental problem in the Earth sciences is increasingly addressed by interdisciplinary studies bridging any number of geophysical observations with geochemical signatures that have been interpreted in terms of a geodynamic origin [e.g., *Hofmann*, 2003]. In early attempts to compare geochemistry and seismic velocities [e.g., *Castillo*, 1988], it was recognized qualitatively that a regional geochemical anomaly in the southern hemisphere (coined Dupal anomaly by *Hart* [1984]) is located over the seismically slow, lower mantle structures under the South Pacific and Africa. This correlation is based on geochemical signatures observed at the Earth's surface and seismic velocities in the lower mantle, assuming a vertical connection between the two observations. More recently, integrated geochemical and geophysical observations on a global scale have been explained with mantle models that

suggest some form of vertical stratification, or reservoir isolation [e.g., *Kellogg et al.*, 1999; *Becker et al.*, 1999; *Albarède and van der Hilst*, 2002; *Hofmann*, 2003; *Labrosse et al.*, 2007]. In many of these models, fractions of the lower mantle are suggested to host the material observed at hot spot volcanoes. By focusing on observations at a given set of hot spot locations, vertical relationships have been pointed out between hot spot locations or related large igneous province eruptions and the edges or large gradients in lower mantle seismic velocity structures [*Thorne et al.*, 2004; *Torsvik et al.*, 2008]. Despite such suggested relationships, statistics has also been used to argue that hot spot locations do not significantly correlate with anomalies in seismic tomography [e.g., *Ray and Anderson*, 1994; *Wen and Anderson*, 1997]. However, highly significant correlations between tomography, convection-affected plume conduits [*Steinberger and Antretter*, 2006] and surface hot spots have been found [*Boschi et al.*, 2007, 2008], suggesting a deep mantle origin for some hot spots. Such results also imply that despite the mismatch between the resolution of seismic tomography ($\sim$1000 km) and the likely dimension of plume conduits ($\sim$100 km), a number of plumes appear to have seismic anomalies associated with them. *Boschi et al.* [2007] found plume-related anomalies by searching for anomalous velocities downward below hot spots, and they suggest that their merging at depth may represent under-resolved plume clusters within the lowermost part of the Pacific and African large seismic velocity structures [e.g., *Schubert et al.*, 2004]. Moreover, the correlation of hot spot-connected plume conduits and seismic velocity anomalies are significant compared to correlations of random conduit locations and seismic velocities [*Boschi et al.*, 2008].

[3] The alternative to a global approach is to focus on individual hot spot settings, with potentially higher resolution. Lower mantle-rooted plumes have been inferred from finite frequency tomography [*Montelli et al.*, 2006] and high-density, regional seismic network data [*Wolfe et al.*, 2009], which would imply transport from the deep mantle at hot spots. However, it is likely that not all hot spots result from deep mantle plumes, which led *Courtillot et al.* [2003] to distinguish three types of hot spots based on a scoring system that evaluates the presence of a linear volcanic chain, a flood basalt province at its inception, a large buoyancy flux, He isotope anomalies, and low shear wave velocities. Based on these criteria, only seven hot spots result from plumes from the core-mantle boundary, while other hot spots result from upper mantle plumes, or plate cracking. *Anderson* [2005] expanded on this scoring approach by evaluating the likelihood of either plume-driven or plate-driven hot spot volcanism, as part of the ongoing "plume debate."

[4] The results of *Courtillot et al.* [2003] and *Anderson* [2005] are mainly based on qualitative evaluation of five and twelve types of observations, respectively, and other studies have also only involved different small sets of observations. Here, a much broader set of parameters is investigated, correlating 27 geological and geophysical hot spot/plume parameters with each other, while testing for significance. Our results reveal $\sim$ten significant correlations which we interpret in terms of the origin of deeply rooted plumes and mantle dynamics in general.

2. Correlation of 27 Parameters for 44 Hot Spots

[5] Values for all the parameters were compiled for the 44 different continental and oceanic hot spots of *Steinberger* [2000], although not all types of parameters are available for each hot spot. Correlations of inferred plume conduits deflected by modeled mantle flow provide better correlations with seismic models than vertical relationships [e.g., *Boschi et al.*, 2007, 2008], and therefore locations along advected conduits are used here to evaluate geophysical parameters. We correlated each type of parameter against all other parameters for all hot spots, and assessed the correlation significance by Student's t test, a Spearman rank test, and a Monte Carlo simulation, as described below. In the following sections we will discuss correlations and anti-correlations that are significant according to our estimates, and we will not discuss the trivial correlations between different seismic velocity models or correlations between isotope ratios and geochemical affinities that were derived from these data.

2.1. Description of the Parameters

[6] The data used for this study were compiled from a range of sources into a table with single entries per hot spot location, following *Davies* [1988], *Sleep* [1990], *Steinberger* [2000], *Becker and Boschi* [2002], *Montelli et al.* [2006], *Steinberger and Antretter* [2006], *Boschi et al.* [2007, 2008], *Courtier et al.* [2007], *Simmons et al.* [2007], and *Lee*

Table 1 (Sample). Geologic and Geophysical Observations at Hot Spot Locations[a] [The full Table 1 is available in the HTML version of this article]

Location	Latitude	Longitude	Age (Ma)	B_{Stein}	B_{Sleep}	T_P	W_{TZ} (km)	$^{143}Nd/^{144}Nd$	$^{206}Pb/^{204}Pb$
Azores (Pico)	38.5	−28.4	100	1.2	1.1	1443	239	0.51262	19.987
Balleny (Buckle Island)	−66.8	163.3	36	n.d.	n.d.	n.d.	n.d.	0.51296	19.762
Bowie	53	−135	28	0.6	0.3	n.d.	n.d.	0.51306	18.803
Cameroon (Mt.)	4.2	9.2	31	n.d.	n.d.	n.d.	n.d.	0.51277	20.368
Canary	28	−18	65	1	1	1473	238	0.51285	20.205
Cape Verde	15	−24	20	1.1	1.6	n.d.	n.d.	0.51279	19.199
Caroline	5	164	80	1.6	1.6	n.d.	n.d.	0.51296	18.573
Cobb (Axial Smt.)	46	−130	43	0.3	0.3	n.d.	n.d.	n.d.	n.d.
Comores (Karthala)	−11.8	43.3	63	n.d.	n.d.	n.d.	n.d.	0.51288	20.418
Darfur	13	24	140	0.4	n.d.	n.d.	n.d.	n.d.	n.d.
East Africa	6	34	40	1.1	1.2	n.d.	n.d.	n.d.	n.d.
East Australia	−38	143	50	0.9	0.9	n.d.	n.d.	n.d.	n.d.
Easter Islands	−27.1	−109.3	68	2.1	3.3	1462	246	0.51298	19.308
Eifel	50	7	40	n.d.	n.d.	n.d.	n.d.	n.d.	n.d.
Fernando	−4	−32	70	0.7	0.5	n.d.	n.d.	0.51271	19.145
Galapagos (Fern.I.)	−0.4	−91.5	85	1.4	1	1431	226	0.51291	20.002
Guadelupe	27	−113	25	0.3	0.3	n.d.	n.d.	0.51294	20.303
Hawaii (Kilauea)	19.4	−155.3	100	8.3	8.7	1499	235	0.51267	17.686
Hoggar	23	6	20	0.6	0.9	n.d.	n.d.	n.d.	n.d.
Iceland	65	−19	60	1.2	1.4	1452	238	0.51297	19.19
Jan Mayen (Beerenberg)	71.1	−8.2	210	0.6	n.d.	n.d.	n.d.	0.51285	18.709
Juan Fernandez	−34	−82	30	1.7	1.6	1501	242	0.51288	19.094
Kerguelen	−49	69	117	0.9	0.5	n.d.	n.d.	0.5125	18.054
Lord Howe	−33	159	50	0.9	n.d.	n.d.	n.d.	n.d.	n.d.
Louisville	−51	−138	120	3	0.9	n.d.	n.d.	0.51285	19.3
Macdonald (Smt.)	−29	−140.2	120	3.6	3.3	n.d.	n.d.	0.5129	21.89
Marion Island	−46.9	37.8	195	n.d.	n.d.	n.d.	n.d.	0.51288	18.56
Marquesas	−11	−138	9	3.9	3.3	1500	239	0.51274	19.15
Meteor	−52	1	120	0.5	0.5	n.d.	n.d.	n.d.	n.d.
New England	29	−32	120	0.4	n.d.	n.d.	n.d.	n.d.	n.d.
Pitcairn	−25	−129	8	2.5	3.3	1453	229	0.51244	17.611
Raton	37	−104	20	n.d.	n.d.	n.d.	n.d.	n.d.	n.d.
Reunion	−21.2	55.7	67	1.4	1.9	1501	238	0.51283	18.994
Samoa	−15	−168	14	1.6	1.6	1480	235	0.51251	19.23
San Felix	−26	−80	30	1.9	1.6	n.d.	n.d.	0.51255	19.312
Socorro Island	18.7	−111	25	0.5	n.d.	n.d.	n.d.	n.d.	n.d.
St Helena	−18	−10	100	0.4	0.5	n.d.	n.d.	0.51287	20.96
Tahiti (Mehetia)	−17.9	−148.1	5	4.5	3.3	1476	233	0.51259	19.288
Tasmanid	−39	156	50	0.9	0.9	n.d.	n.d.	n.d.	n.d.
Tibesti	21	17	80	0.3	n.d.	n.d.	n.d.	n.d.	n.d.
Trindade (Martin Vas)	−20.5	−28.8	120	0.7	n.d.	n.d.	n.d.	0.51277	19.143
Tristan	−38	−11	125	1	1.7	n.d.	n.d.	0.51247	18.482
Vema	−33	4	40	0.4	n.d.	n.d.	n.d.	n.d.	n.d.
Yellowstone	44.6	−110.5	15	1.5	1.5	n.d.	n.d.	n.d.	n.d.

[a]Key to the observations: Latitude and longitude for current hot spots, age range of the hot spot (age [Ma]) [*Davies*, 1988], potential temperature (Tp) [*Courtier et al.*, 2007], and transition zone thickness (W_{TZ}) [*Courtier et al.*, 2007]; buoyancy flux estimates (B_{Stein} and B_{Sleep}) [*Davies*, 1988, *Sleep*, 1990], most extreme lava isotopic compositions for each hot spot ($^{143}Nd/^{144}Nd$, $^{206}Pb/^{204}Pb$, $^{87}Sr/^{86}Sr$ from the GEOROC database); proportion of geochemical mantle component that each hot spot has the closest affinity for [*Konter et al.*, 2008] based on the GEOROC isotopic compositions (PCA% EM1, EM2, HIMU and C), proportions of independent components [*Iwamori and Albarède*, 2008] derived from isotopic compositions (IC1, IC2), seismic velocity anomalies at the core-mantle boundary (δVs), absolute geographical gradients in seismic velocity at the core-mantle boundary ($|\nabla(\delta Vs)|$), plume depth extent [*Boschi et al.*, 2007, 2008] (δ), and seismic velocity anomalies at 200 km depth (δVs), all for three different seismic models: Pri-S05 [*Montelli et al.*, 2006], TX2009 [*Simmons et al.*, 2007], and SMEAN [*Becker and Boschi*, 2002]; distance to the closest continent computedas great circle distance on a sphere from given hot spot locations and the intermediate resolution coastlines of Generic Mapping Tools [*Wessel and Smith*, 1991]. n.d.: no data available.

et al. [2009]. For most geophysical parameters, single observations are extracted from a global data set at the relevant latitude and longitude of the hot spot's conduit for a particular depth. A brief description of the included parameters follows, while detailed sources are provided in Table 1.

[7] The age corresponds to the time since a hot spot's first activity, and this is defined by a

radiometric age for the oldest volcano in a given volcanic chain. Buoyancy flux refers to an estimate of the flux of buoyantly rising material in the plume, which is generally estimated based on topography, geoid and heat flow. The potential temperature represents the temperature of the mantle considered if it were adiabatically decompressed to the Earth's surface. Transition zone width is the vertical distance between the actual depths of the 440 km and 660 km discontinuity, as they are affected by changes in temperature through the Clapeyron slope of the relevant phase changes. We also include the velocity anomaly, velocity gradient, and plume depth extent extracted from three seismic tomography models that were previously processed for comparison by *Boschi et al.* [2007, 2008]. Based on this previous work, the velocity anomalies considered here for all three seismic models are defined in percent with respect to PREM [*Dziewonski and Anderson*, 1981]. The velocity gradient is calculated as the horizontal gradient in velocity anomalies, such that high gradients should correspond to the edges of large seismic velocity anomaly structures. Plume depth extent describes how deep a slow seismic velocity anomaly can be traced underneath a hot spot into the lower mantle along a plume conduit as inferred from convection modeling (as in Figure 14 of *Boschi et al.* [2007]). In addition to the seismic model data, we also computed the distance (in degrees) between the hot spot locations and the closest continent. For this purpose, the intermediate resolution coastline data set of the Generic Mapping Tools [*Wessel and Smith*, 1991] was used, limiting the data to land areas larger than 250,000 km^2 in order to exclude particularly hot spot and island arc volcanoes. The shortest great circle distance to a coastline is used here as the distance to the closest continent, for each hot spot.

[8] For all parameters discussed above, one value can be obtained for each hot spot location, in contrast to geochemical data. Since a range of samples is commonly available per hot spot, here the most extreme samples were chosen from a data set compiled from the GEOROC geochemistry database (http://georoc.mpch-mainz.gwdg.de). Isotopic compositions were compiled for samples with a whole rock composition that is basaltic. Only samples with combined Sr, Nd, and Pb isotope analysis performed on the same sample were used. This combination of isotopes is necessary to allow correlation with both the raw data and with recognized geochemical end-members. Only oceanic hot spots are considered here for their isotopic composition, since all continental hot spots suffer from the potential of continental crustal contamination. Since the incorporation of continental material into rising melts is not directly related to the origin of these melts, inclusion of data with a shallow crustal contribution would render any conclusions about correlations with deep geophysical observations invalid. For the available oceanic hot spots we follow two approaches here, first estimating the end-member each sample has the closest affinity for [*Konter et al.*, 2008], where the end-members were originally found through principal component analysis. Second, we decompose each sample composition in terms of its independent components [*Iwamori and Albarède*, 2008].

[9] Estimating the affinity is performed by comparing where each sample is located within the total scatter of isotopic data. The geochemical components can be identified using radiogenic isotope compositions of erupted lavas, obtained for all the hot spots from the GEOROC geochemistry database. Principal component analysis of combined mid ocean ridges and hot spots data (^{87}Sr/^{86}Sr, ^{143}Nd/^{144}Nd, ^{206}Pb/^{204}Pb, ^{207}Pb/^{204}Pb, ^{208}Pb/^{204}Pb) has revealed that the data variation in the three-dimensional space defined by the principal components ^{87}Sr/^{86}Sr, ^{143}Nd/^{144}Nd, and ^{206}Pb/^{204}Pb requires at least four different components [*Allègre et al.*, 1987], the mantle components HIMU, EM1, EM2, and DMM. These components define the apices of the geochemical mantle tetrahedron, which encloses all the data in ^{87}Sr/^{86}Sr, ^{143}Nd/^{144}Nd, and ^{206}Pb/^{204}Pb isotope space [*Zindler and Hart*, 1986; *Hart et al.*, 1992]. An additional mantle component is also included, intermediate in ^{87}Sr/^{86}Sr, ^{143}Nd/^{144}Nd, and ^{206}Pb/^{204}Pb isotope compositions, but distinct in ^{3}He/^{4}He signature (i.e., FOZO or C of *Hart et al.* [1992] and *Hanan and Graham* [1996]). This component is recognized as the intersection of all data arrays of the different oceanic volcanic systems. We use the technique of *Konter et al.* [2008] to estimate the affinity, which uses a point estimate of the intermediate component (^{87}Sr/^{86}Sr: 0.703303, ^{143}Nd/^{144}Nd: 0.512950, ^{206}Pb/^{204}Pb: 19.238; referred to as C hereafter) instead of the ranges given for C or FOZO. From this intermediate point, tie-lines can be drawn to the other mantle components, and we can define which tie-line and mantle component each sample has the strongest affinity for [*Konter et al.*, 2008]. Each sample is projected onto tielines between the internal C component and the end-members EM1, EM2, HIMU and DMM. Subsequently, the distance of the sample along each tieline

is expressed as a percentage of the total distance from C to the end-member. The tieline along which this percentage is the highest is assumed to reflect the strongest affinity. Each hot spot is then scored with the affinity of the most extreme sample.

[10] Our method can recover percentages of all end-member affinities as a result of the projection approach. However, the compositional data of each hot spot form elongated arrays that trend from C or FOZO toward the end-member of the strongest affinity, while trending away from the other end-members. Therefore, using projected compositions along the other tielines would misrepresent the trend of the compositional array, and we only use the strongest affinity to compare to other parameters.

[11] A different way to represent the chemical compositions is with the use of independent component analysis [*Iwamori and Albarède*, 2008], where the data is mapped onto two new, independent axes that are aligned with the maximum variation in the data. The two major independent components found for a large data set of oceanic lavas correspond to a component that distinguishes mid oceanic ridge lavas from hot spot lavas, and the geographic anomaly in composition known as the Dupal anomaly [*Hart*, 1984]. The contribution of both these components can thus be evaluated for each sample using the independent component analysis. Since the first component distinguishes mid oceanic ridge lavas from intraplate lavas, and the locations considered here are all intraplate volcanic systems, we might expect to see little correlation with this component. The second component, the Dupal anomaly, is identified by the distance of a sample from the best fit line through the Pb isotope data of all available oceanic lavas of the Northern hemisphere (NHRL [*Hart*, 1984]). This type of scatter is not truly evaluated by either approach taken here [*Konter et al.*, 2008; *Iwamori and Albarède*, 2008], and we might expect not to find any clear correlations for this component.

2.2. Correlations and an Estimate of Their Significance

[12] All observations were correlated and the results are shown in Figures 1 and 2. In order to test which correlations are statistically significant, several different techniques were applied. The color-coding in Figure 1 shows the linear (Pearson) correlation, r value, while the statistical significance of that correlation is given as percent probability (from Student's t test, $N - 2$ degrees of freedom, where N is the number of observations). In an alternative approach, the Spearman rank correlation coefficient can be calculated (Figure 2). This technique shows overall similar results to the r values and their significance levels, but should be less sensitive to outliers. In most cases the difference between the significance of the correlations (t-test) only differs by a few percent, although some correlations are different by up to ~20%. This approach also highlights the degree of robustness of significant correlations between the same geochemical components and the seismic parameters as the standard r value approach.

[13] To test deviations from the assumptions inherent in Student's t test, the significance of the r values presented in Figure 1 was also evaluated using a Monte Carlo simulation. Two different approaches were taken, both for EM1 correlations: (1) randomizing the order of the geochemical data with respect to the actual order of locations and (2) assigning random values at each location. In each case, r values were calculated for one thousand sets of random data. The mean r value for each simulation is zero, while two standard deviations range to an absolute r value of ~0.73 for both simulations (Figure 3). Roughly, these simulations suggest that t-test significance values greater than ~91% are significant. Since other geochemical end-members may have a different number of observations, the same calculations were performed for EM2, suggesting the threshold lies at an absolute r value of ~0.8 for these correlations. This approach shows that there are only a few correlations that are significantly different from an expected random correlation, and these are discussed below.

3. Results

[14] A number of strong correlations and anti-correlations are found (Figures 1 and 2). In particular, significant correlations are detected for the mantle component for which a sample has the strongest affinity (EM1, EM2, HIMU affinity), and the tomographically based depth extent of the inferred plumes feeding the volcanoes [*Boschi et al.*, 2007, 2008]. In addition, anti-correlations are found for the mantle component for which a sample has the strongest affinity (EM1, C affinity) and shallow mantle S wave velocity anomalies in all three seismic tomography models considered. In contrast to the end-member affinity, the other compositional representations including the main component found by independent components analysis [*Iwamori*

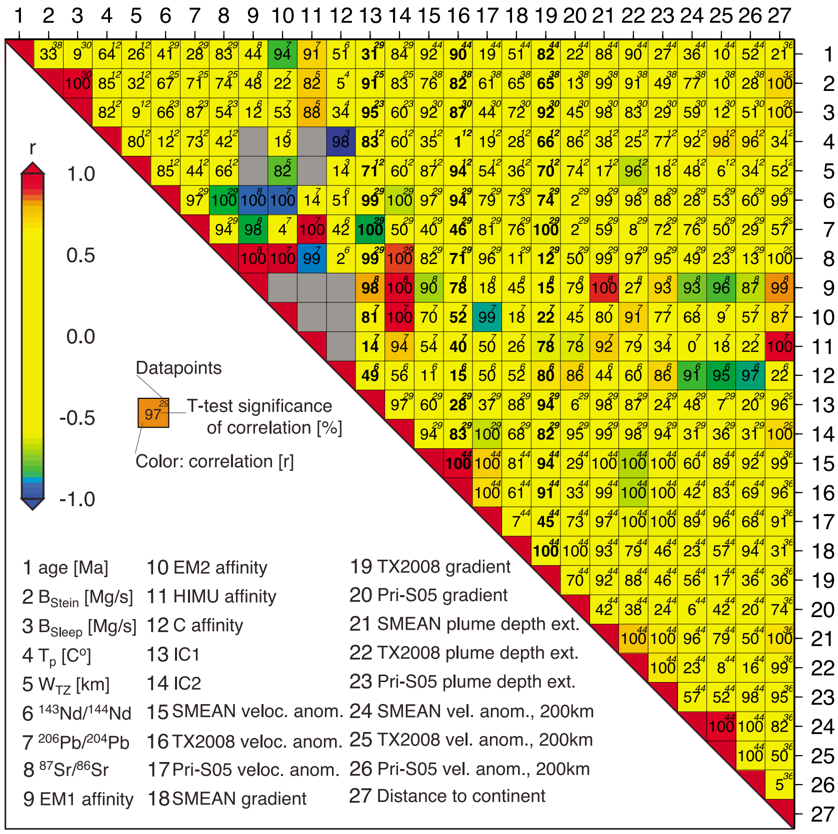

Figure 1. Correlation matrix of observations for all the hot spot locations, showing student's t-test correlation significance. The color corresponds to the linear (Pearson) correlation coefficient, and the numbers refer to the significance of the correlation and the number of samples used in the correlation (italicized). Key to the observations correlated: age range of the hot spot (age [Ma]), potential temperature (Tp), and transition zone thickness (W_{TZ}) [*Davies*, 1988; *Courtier et al.*, 2007]; buoyancy flux estimates (B_{Stein} and B_{Sleep}) [*Davies*, 1988; *Sleep*, 1990; *Steinberger and Antretter*, 2006]; most extreme lava isotopic compositions for each hot spot ($^{143}Nd/^{144}Nd$, $^{206}Pb/^{204}Pb$, $^{87}Sr/^{86}Sr$ from the GEOROC database); percentage of geochemical mantle component that each hot spot has the closest affinity for [*Konter et al.*, 2008] based on the same isotopic compositions (EM1, EM2, HIMU and C affinity); proportions of independent components [*Iwamori and Albarède*, 2008] derived from isotopic compositions (IC1, IC2); seismic velocity anomalies at the core-mantle boundary (δv_S (%) of seismic models Pri-S05 [*Montelli et al.*, 2006], TX2008 [*Simmons et al.*, 2007], SMEAN [*Becker and Boschi*, 2002]); absolute geographical gradients in seismic velocity at the core-mantle boundary ($|\nabla(\delta v_S)|$); plume depth extent [*Boschi et al.*, 2007, 2008] as traced in different seismic models (δ); and seismic velocity anomalies at 200 km depth (δv_S); calculated distance (°) from the hot spot to the closest continent.

and Albarède, 2008] and the raw isotopic compositions do not seem to correlate or anti-correlate significantly.

[15] To us, the most intriguing correlation we report suggests that the advected plume depth extent in seismic *S* velocity models not only correlates with hot spot locations [*Boschi et al.*, 2007, 2008] but also with geochemical compositions (Figures 1, 2, and 4). The geochemical EM1 component shows some of the strongest correlations with plume depth extent, and in addition it shows anti-correlations with *S* velocity models at 200 km depth. The other geochemical components show no correlation with *S* velocities at 200 km. The C component is the only exception, showing anti-correlations with *S* velocity models at 200 km depth, but no correlation with plume depth extent. The EM2 component is the only component that shows a correlation with *S* wave velocity at the core-mantle boundary (CMB), but only for one of the seismic models [*Montelli et al.*, 2006]. Significant correlations are also found between EM1 affinity or to a lesser extent HIMU affinity (for *r* but not r_{Spear}) and distance to the closest continent. This distance also correlates significantly with buoyancy flux. However, we note that the distance to the closest continent does not distinguish between active and passive continental margins, which is important when considering any relationship between observations at hot

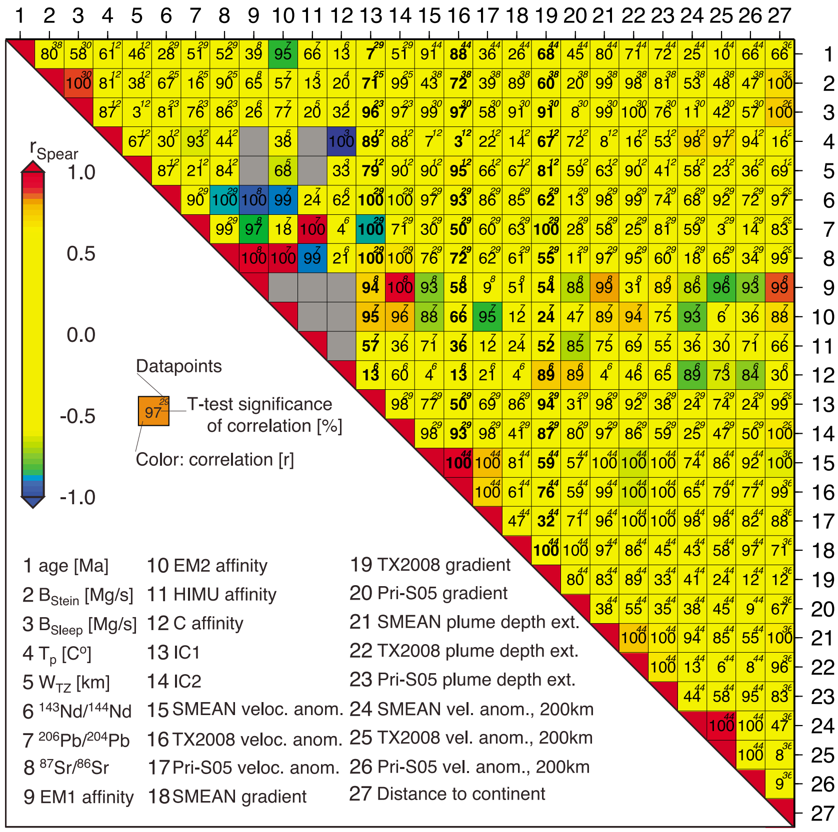

Figure 2. Correlation matrix of observations for all the hot spot locations, showing Spearman rank correlation coefficients, all else as in Figure 1. The color corresponds to the correlation coefficient, and the numbers refer to the significance of the correlation and the number of samples used in the correlation (italicized). For the key to the numbered observations, see Figure 1.

spots and continents. Furthermore, our inferred velocity gradients do not produce strong correlations with other observations, while multiple studies have pointed out that the location of a number of hot spots correspond to the edges of the large seismic velocity structures in the Pacific and under Africa [e.g., *Thorne et al.*, 2004; *Torsvik et al.*, 2008]. In summary, it appears all geochemical components can be traced to greater depth (plume depth extent), but only EM1 also involves a source in the shallow mantle.

[16] The correlations for other parameters are less significant, but we will briefly discuss results for correlations near the significance level. The age parameter (time span of activity of the volcanic chain related to each hot spot) only correlates with geochemical component EM2 and HIMU. These are likely biased by some of the older submarine volcanoes in the western Pacific [*Konter et al.*, 2008]. The buoyancy flux correlates weakly with plume depth extent and provides an estimate of the supply from the mantle. Potential temperature estimates [*Lee et al.*, 2009] only show a negative correlation with C and somewhat surprising positive correlations with shallow *S* wave velocity anomalies. However, at this depth (200 km) the tomography models are dominated by velocities in the lithosphere and slow anomalies associated with mid oceanic ridges. Therefore, temperatures at near-ridge hot spots are effectively correlated with ridge seismic signatures. Hot spots further away generate melt under a thicker lithosphere, requiring either higher temperatures, or significant volatile content to enable melting to generate volcanic chains. Next, weak correlation between transition zone width and CMB velocity anomalies exist for only one of the seismic models, where thicker zones are expected for cold regions (subducting plates), and thin zones for areas of hot potentially upwelling mantle. Finally, the EM2 component shows a significant anti-correlation with seismic velocities at the CMB for the model by *Montelli et al.* [2006], while no significant anti-correlation is found for the other seismic models (EM1 is just

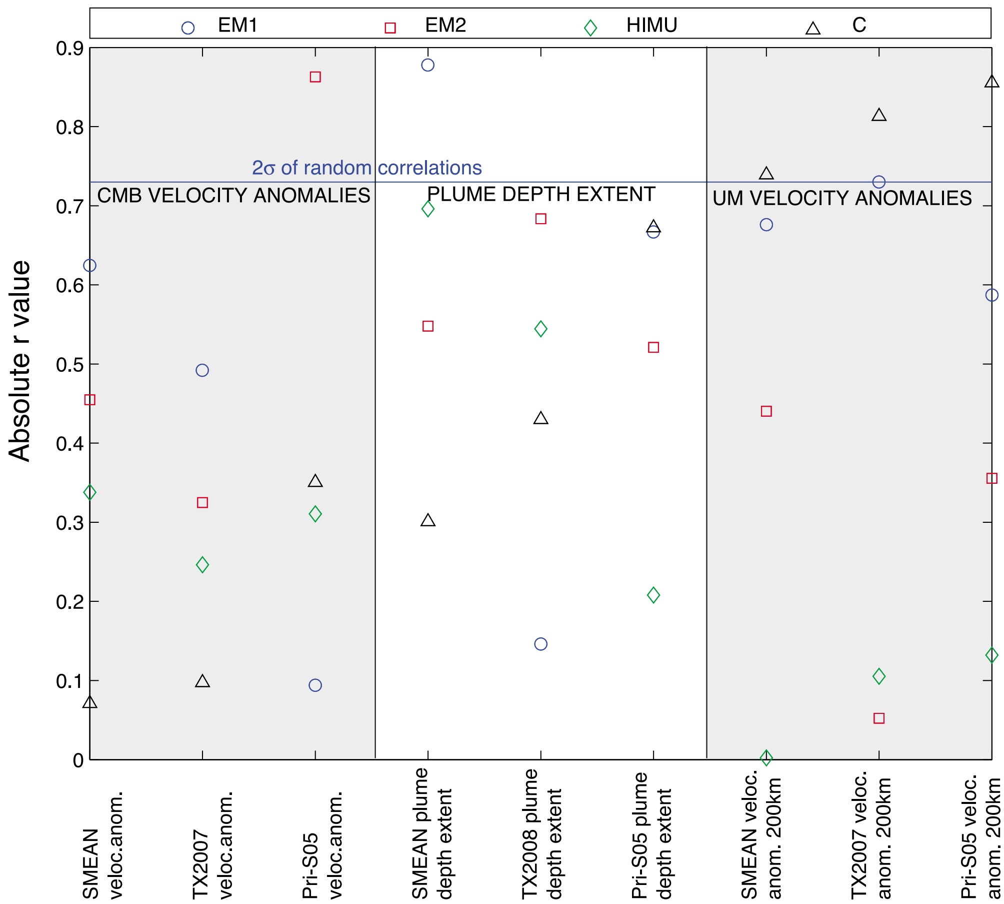

Figure 3. Comparison of correlation coefficients of hot spots with a particular geochemical affinity correlated with three different seismic models for core-mantle boundary velocity anomalies (δv_S), plume depth extent (δ), and upper mantle (200 km) velocity anomalies (δv_S). Blue line shows two standard deviations of random correlations from Monte Carlo simulations for EM1.

below significance). A related observation that is robust is the lack of anti-correlations for the other mantle components with any of the seismic models. This might be due to the hot spot sources sampling more than the four pure mantle components, instead sampling an array of various similar components, as suggested for EM sources [*Class et al.*, 2009], resulting in different values for the affinities.

[17] Alternatively, the lack of anti-correlation may be related to the previously suggested location of hot spots near the edge of slow seismic structures in the deep mantle [e.g., *Thorne et al.*, 2004], which implies a source location away from the seismically slowest mantle. However, advected conduit source locations do not correlate significantly with large gradients in seismic velocity anomaly [*Boschi et al.*, 2007], nor do the velocity gradients correlate significantly with any of the parameters considered here. Since these results argue against existing models, we discuss these non-correlations further in section 5. Other weak correlations near the signifi- cance level will, however, not be further discussed.

4. Discussion of Resulting (Anti-)correlations

[18] The study of combined geophysical and geochemical data is a key approach to further our understanding of the dynamic origin of hot spots as well as their source materials. By correlating a large set of parameters for a global hot spot catalog (see Table 1), we find only a subset of these parameters display (anti-)correlations. Particularly, the correlations between some of the geochemical compositions and seismic models stand out; those show the best correlations between the geochemical mantle components and plume depth extent, and not as much (anti-)correlations with slow velocities

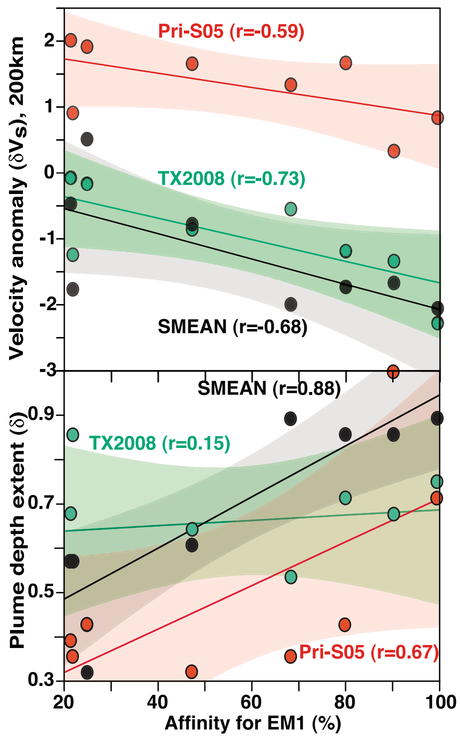

Figure 4. Individual hot spots with high affinity for the EM1 geochemical component show an anti-correlation of affinity for EM1 (percentage) with (top) shear wave speed anomalies at 200 km and (bottom) a weaker correlation with plume depth extent. Correlations are shown for three different seismic models (circles; red for Pri-S05 [*Montelli et al.*, 2006], green for TX2008 [*Simmons et al.*, 2007], and black for SMEAN [*Becker and Boschi*, 2002] S velocity models). Confidence (95%; Working-Hotelling) bands are shown for each correlation.

at the CMB. This implies that the main geochemical mantle components have a deep origin, but potentially not from the CMB. Instead, they may have an origin in a deep layer or structure that extends well above the CMB [e.g., *Kellogg et al.*, 1999], or alternatively there may be a difference between the true convection-affected conduits and the modeled locations used here. A third explanation is that the resolution of global tomographic models in the lower mantle is lower than the expected plume conduit dimensions, and as a result the tomography data yields an undersampled image of the mantle structure. For example, *Schubert et al.* [2004] show that the resolution of seismic tomography decreases quickly in the deepest ~400 km above the CMB, particularly in the areas of the large seismic velocity structures in the Pacific and under Africa, and instead only clusters of plumes may be imaged. Therefore, correlations of individual hot spots and their properties should not be expected with seismic velocity anomalies at the CMB.

[19] In addition to the general result of deeply rooted geochemical components, the EM1 and C component display anti-correlations at shallow depths (200 km) implying that a shallow process or origin is associated with these mantle components. These individual components are discussed below.

4.1. Correlations of the EM1 Geochemical Reservoir

[20] The observed correlation of EM1 with plume depth extent and anti-correlation with shallow velocity anomalies (Figure 4) favor one of several proposed origins for the EM1 mantle component. Its isotopic composition has been explained by shallow incorporation of particularly sub-continental lithospheric mantle, lower crust, deep recycling of ancient pelagic sediment, or metasomatized and subsequently depleted bulk silicate Earth [*Hofmann*, 2003; *Gibson et al.*, 2005; *Class and Le Roex*, 2006; *Regelous et al.*, 2009; *Salters and Sachi-Kocher*, 2010, and references therein]. Our observations are best explained with a model (Figure 5) [*Hawkesworth et al.*, 1986; *Carlson et al.*, 1996; *Milner and le Roex*, 1996; *Peate et al.*, 1999; *Gibson et al.*, 2005; *Class and Le Roex*, 2006] where an upwelling plume (that explains the correlation with plume depth extent) incorporates sub-continental lithospheric mantle in the shallow mantle (which would explain the anti-correlation with *S* velocities at 200 km). If the EM1 composition truly represents continental material, a logical step would seem to consider the distance from continents. However, the correlations with distance to continents are dominated by the hot spots located over the Pacific large low seismic velocity structure, which are the furthest from any continent. These hot spots are also on a plate separated from most continents by subduction zones, which suggests that any potential sub-continental lithospheric mantle or lower crust being sampled likely did not originate from the current continental margins. Instead, an older tectonic event such as the opening and/or closing of the Tethys ocean basin may need to be invoked, demonstrating that a more in-depth study involving plate reconstructions is required to evaluate the relationship between compositions and distances to potential continental sources. Although such an in-depth study is beyond the scope of this paper, we do model pollution of the shallow mantle with sub-continental lithospheric mantle or lower crustal granulite on a purely compositional basis.

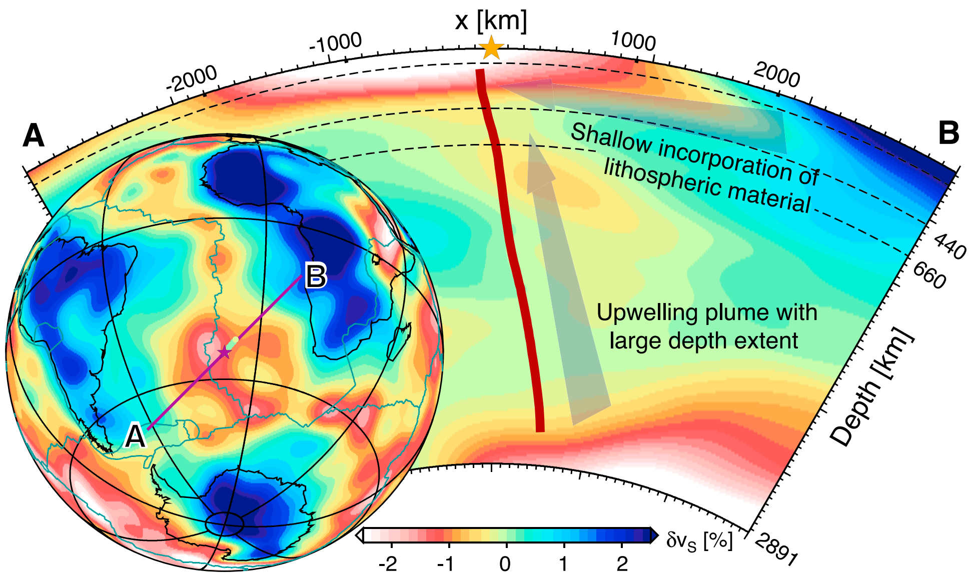

Figure 5. A profile through the SMEAN S velocity model [*Becker and Boschi*, 2002] for the Tristan (EM1) hot spot shows the dynamically predicted conduit (dark red [*Steinberger and Antretter*, 2006; *Boschi et al.*, 2007, 2008]) follows a seismically slow structure in the mantle, suggesting an explanation for the correlation of composition with plume depth extent. In the upper mantle some lithospheric material can be incorporated into the upwelling plume to generate the isotopic composition observed at the surface. The inset shows the location of the profile across the South Atlantic Ocean.

4.2. Modeling the EM1 Geochemical Reservoir

[21] An origin for the EM1 component from continental material that was incorporated into the melt source at shallow depths has been previously proposed by a number of workers, and our correlations agree with this general model. In general, both incorporation of sub-continental lithospheric mantle [*Hawkesworth et al.*, 1986; *Carlson et al.*, 1996; *Milner and le Roex*, 1996; *Peate et al.*, 1999; *Gibson et al.*, 2005; *Class and Le Roex*, 2006], or lower crust [*Hanan et al.*, 2004; *Escrig et al.*, 2005; *Regelous et al.*, 2009] have been proposed to explain the EM1 component observed along the southern Atlantic Ridge, the Tristan-Gough-Walvis hot spot, the Parana-Etendeka flood basalts, and the Australian-Antarctic Discordance. Since the origin of EM1 is still the least constrained in comparison to other mantle components [e.g., *Hart*, 2011], we discuss the significance of our correlations and their implications for the origin of EM1. In particular, the correlation of EM1 affinity with plume depth extent as well as anti-correlation with seismic velocity anomalies in the shallow mantle need to be considered. Since many hot spot chains including the EM1 hot spots Pitcairn, Tristan and Gough show a range in isotopic compositions from FOZO or C toward an end-member (EM1 in this case; Figure 6), the FOZO or C component is likely a common component that is integral to the sampled source components in oceanic volcanism, as suggested by *Hart et al.* [1992] and *Hanan and Graham* [1996]. We consider here the possibility of upwelling mantle with C composition (to explain the correlation with plume depth extent) contaminated with continental mantle or lower crust to provide an EM1 component at shallow depth (to explain the correlation with shallow seismic velocities). This is a more likely scenario than shallow inclusion of a C component into upwelling mantle with EM1 composition, since other hot spots display compositional arrays including the C component, but without the shallow anti-correlation between compositions and seismic velocities. This argument justifies our testing for shallow inclusion of an EM1 component.

[22] Although mixing calculations of mantle melts with continental material have been carried out by many workers, we have carried out a new set of calculations to include both Atlantic and Pacific Ocean hot spots with strong EM1 affinity (see auxiliary material).[1] Furthermore, the recent refinement of the composition for FOZO corresponds to samples from Rurutu (Cook-Austral Islands), providing an

[1] Auxiliary materials are available in the HTML. doi:10.1029/2011GC003923.

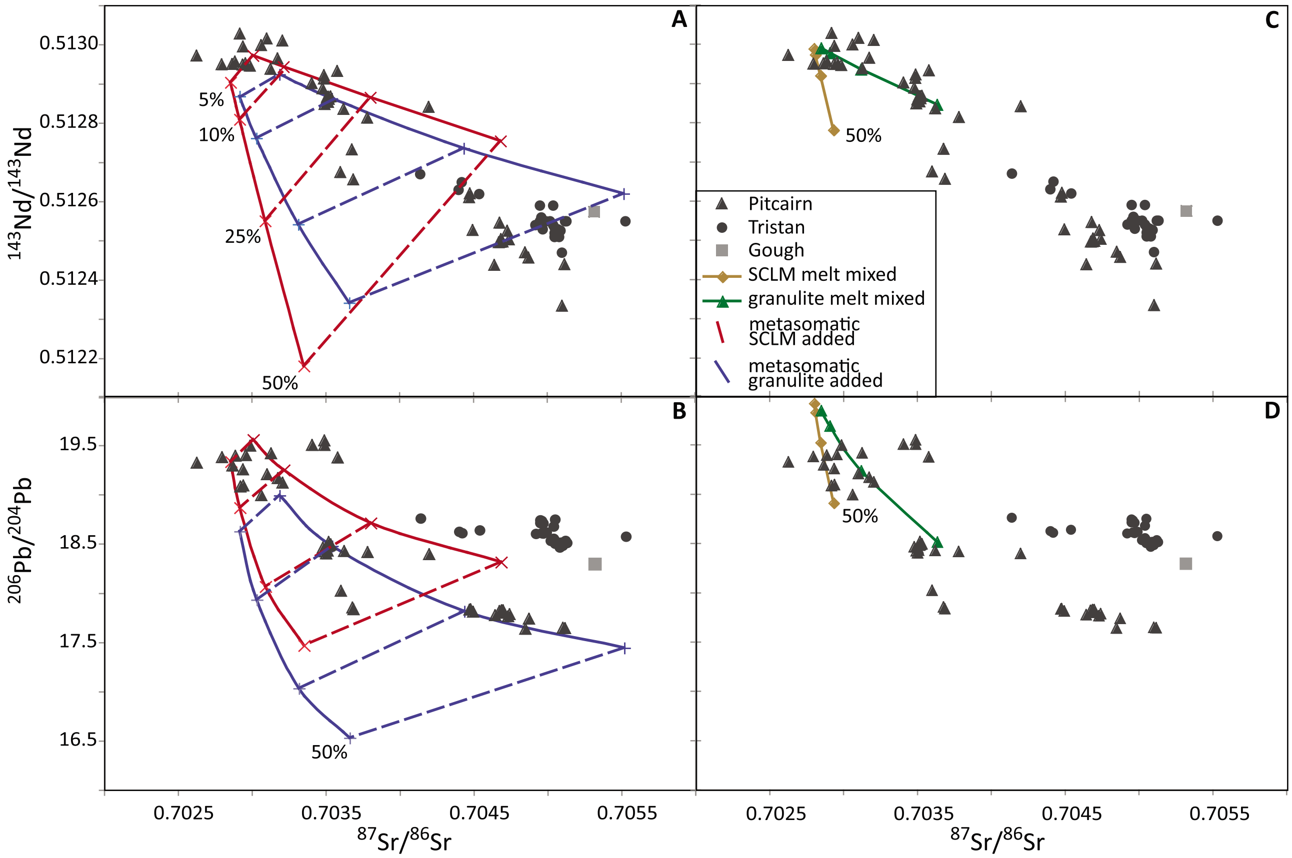

Figure 6. Two component mixing models for EM1, showing calculations for contributions from sub-continental lithospheric mantle or granulite to a composition corresponding to component C. (a) Nd-Sr isotope data for EM1 hot spots and modeled mixing ranges for metasomatic addition of sub-continental lithospheric mantle melt (red lines) or granulite melt (blue lines) to C. Two different samples for both sub-continental lithospheric mantle and granulite were used to demonstrate range in possible compositions, where dashed lines indicate fraction of sub-continental lithospheric mantle or granulite added (in percent). (b) Same mixing models as Figure 6a shown for Pb-Sr isotope compositions. (c) Mixing calculations for mixing of sub-continental lithospheric mantle (brown) or granulite (green) melt with melt of C mantle. Only one sample mixture is shown for each, since they adequately demonstrate nearly pure sub-continental lithospheric mantle or granulite will be necessary to explain observed extreme EM1 lavas. (d) Same calculation as Figure 6c shown for Pb-Sr isotope compositions.

opportunity to estimate trace element compositions in the intermediate isotopic component FOZO and/or C. These concentrations are higher than previously used [e.g., *Hawkesworth et al.*, 1986; *Gibson et al.*, 2005], resulting in larger required contributions from the continental component, up to 50% of either sub-continental lithospheric mantle or granulite melt added to peridotite with average composition, here chosen as C. The alternative of mixing melts of either lithospheric mantle or granulite with a peridotite melt with a composition like the C component would require nearly pure sub-continental lithospheric mantle or granulite to explain extreme EM1 lavas. Either mantle or crustal continental material may have been incorporated, and indeed it has even been proposed that both components and potentially an EM1 plume component may be sampled by different volcanic systems in the south Atlantic Ocean basin [e.g., *Gibson et al.*, 2005; *Regelous et al.*, 2009; *Class and Le Roex*, 2011]. Incorporation of sub-continental lithospheric mantle seems to fit slightly better to the data (Figure 3), and the Walvis Ridge EM1 source can be traced to cratonic sub-continental lithospheric mantle with EM1 composition. We, therefore, consider sub-continental lithospheric mantle likely to be the major source for the EM1 component, although the data scatter suggests some variation in the EM1 mixing component that does not allow us to exclude lower crustal contributions. Thermal erosion of sub-continental lithospheric

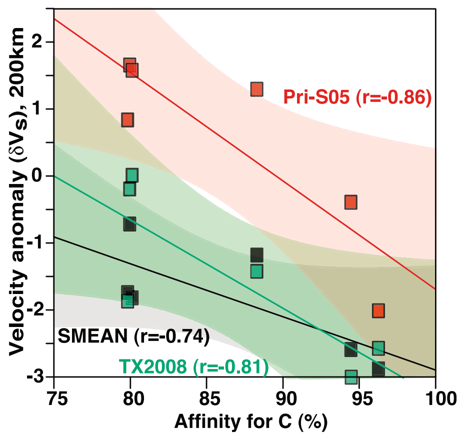

Figure 7. Negative correlation of individual hot spots with an affinity for the C geochemical component with shear wave speed anomalies at 200 km (squares; red for Pri-S05 [*Montelli et al.*, 2006], green for TX2008 [*Simmons et al.*, 2007], and black for SMEAN [*Becker and Boschi*, 2002] models). Confidence (95%; Working-Hotelling) bands are shown for each correlation.

mantle has been proposed as the most likely process to generate EM1 material that can be incorporated. Increased temperature due to thermal erosion or possibly partial melting of sub-continental lithospheric mantle can explain the anti-correlation with shallow seismic velocities, and fits well with the metasomatic addition model. The integration of geophysical and geochemical observations therefore clarifies the possible origin of EM1.

4.3. Correlations of the C Geochemical Component

[23] In contrast to the other mantle components, the geochemical C component only shows a strong anti-correlation with shallow velocity anomalies (Figure 7). Although most isotopic arrays of oceanic volcanism intersect at this component [*Hart et al.*, 1992; *Hanan and Graham*, 1996], they do not all display an anti-correlation in the shallow mantle. Therefore, the anti-correlation may not reflect the direct presence of C, but rather an indirect effect of its presence such as a higher degree of partial melt. Such a difference in degree of melt might be expected from the more enriched radiogenic isotope compositions compared to surrounding MORB upper mantle, which requires time-integrated trace element enrichment, suggesting a more fertile source. One caveat is the fact that the C component is commonly recognized by its He isotope composition [*Hanan and Graham*, 1996], implying that correlations should be made based on He isotopes before strong statements can be made about the location of C in the mantle.

5. Relevance of Non-correlations

[24] Another aspect of our results concerns the lack of (anti-)correlations for some parameters. Particularly, it has recently been pointed out that a large number of hot spots and the original eruptive location of large igneous provinces (reconstructed with absolute plate motion) occur near the edges of the large, low velocity structures in the lower mantle [*Thorne et al.*, 2004; *Torsvik et al.*, 2008]. Since these edges correspond to locations where the horizontal gradient in velocity should be large, we correlated all our parameters against the gradients in the different velocity models. However, there are no significant (anti-)correlations with these gradients and conduit locations [*Boschi et al.*, 2007] or parameters considered here. There are a number of potential reasons for this disagreement with previous studies: (1) a plume source "at the edges" of the low velocity provinces does not require that sources are located over the largest velocity gradients, but rather at some iso-velocity contour [*Torsvik et al.*, 2008], which was not considered here. (2) We used convection-affected conduits while other studies correlate vertically between surface and CMB. (3) As suggested by *Boschi et al.* [2007], a plume may form at a high gradient [e.g., *McNamara and Zhong*, 2005; *Torsvik et al.*, 2006], but then be advected to slow velocity regions. This is our preferred explanation, and if the location of the plume base is indeed time dependent, it is not the hot spot location but the time-dependence of its base that can explain the lack of an anti-correlation between seismic velocity anomaly gradients and the end-member affinities (except EM2).

6. Conclusion

[25] Among all of the hot spot-associated correlations we compute, the highly significant ones are those of the EM1 component with both shallow seismic velocities and the depth extent to which a hot spot source can be traced with seismic tomography. Although correlation does not imply causality, our model for EM1 is additionally supported by geophysical and geodynamical observations. These relationships provide the first integrated evidence for buoyantly rising plumes of mantle material (depth extent correlation), incorporating thermally eroded continental material in the shallow mantle (anti-correlation with shallow seismic

velocities). By modeling mixtures of either subcontinental lithospheric mantle or lower crustal granulite with peridotite of average mantle composition (C component), we demonstrate the suitability of these components and thereby the feasibility of the model. Our findings imply that upwelling plumes rise from the deep mantle, which would constitute significant mass transport between the lower and upper mantle. Thus, these findings contribute to our understanding of mantle dynamics, while explaining the origin of a significantly debated mantle compositional end-member (enriched mantle; EM1).

Acknowledgments

[26] We thank all geochemists and seismologists who share their data and models in electronic form, GEOROC for their archival efforts, and B. Steinberger and C.-T. Lee for sharing their respective hot spot-associated parameter databases. We thank F. Albarède, C.-T. Lee, L. Boschi, B. Steinberger, and S. Hart for comments and discussions. Rick Carlson and Joel Baker are thanked for their constructive reviews and editorial handling. Compilation of the isotope data set and initial correlations were performed at the 2004 Cooperative Institute for Dynamic Earth Research (CIDER) summer program.

References

Albarède, F., and R. D. van der Hilst (2002), Zoned mantle convection, *Philos. Trans. R. Soc. London, Ser. A*, *360*, 2562–2592, doi:10.1098/rsta.2002.1081.

Allègre, C. J., B. Hamelin, A. Provost, and B. Dupré (1987), Topology in isotopic multispace and origin of mantle chemical heterogeneities, *Earth Planet. Sci. Lett.*, *81*, 319–337, doi:10.1016/0012-821X(87)90120-8.

Anderson, D. L. (2005), Scoring hotspots: The plume and plate paradigms, in *Plates, Plumes, and Paradigms*, edited by G. R. Foulger et al., *GSA Spec. Pap.*, *388*, 31–54.

Becker, T. W., and L. Boschi (2002), A comparison of tomographic and geodynamic mantle models, *Geochem. Geophys. Geosyst.*, *3*(1), 1003, doi:10.1029/2001GC000168.

Becker, T. W., J. B. Kellogg, and R. J. O'Connell (1999), Thermal constraints on the survival of primitive blobs in the lower mantle, *Earth Planet. Sci. Lett.*, *171*, 351–365, doi:10.1016/S0012-821X(99)00160-0.

Boschi, L., T. Becker, and B. Steinberger (2007), Mantle plumes: Dynamic models and seismic images, *Geochem. Geophys. Geosyst.*, *8*, Q10006, doi:10.1029/2007GC001733.

Boschi, L., T. Becker, and B. Steinberger (2008), On the statistical significance of correlations between synthetic mantle plumes and tomographic models, *Phys. Earth Planet. Inter.*, *167*, 230–238, doi:10.1016/j.pepi.2008.03.009.

Carlson, R. W., S. Esperança, and D. P. Svisero (1996), Chemical and Os isotopic study of Cretaceous potassic rocks from Southern Brazil, *Contrib. Mineral. Petrol.*, *125*, 393–405, doi:10.1007/s004100050230.

Castillo, P. (1988), The Dupal anomaly as a trace of the upwelling lower mantle, *Nature*, *336*, 667–670, doi:10.1038/336667a0.

Class, C., and A. Le Roex (2006), Continental material in the shallow oceanic mantle—How does it get there?, *Geology*, *34*, 129–132, doi:10.1130/G21943.1.

Class, C., and A. Le Roex (2011), South Atlantic DUPAL anomaly—Dynamic and compositional evidence against a recent shallow origin, *Earth Planet. Sci. Lett.*, *305*, 92–102, doi:10.1016/j.epsl.2011.02.036.

Class, C., S. L. Goldstein, and S. B. Shirey (2009), Osmium isotopes in Grande Comore lavas: A new extreme among a spectrum of EM-type mantle endmembers, *Earth Planet. Sci. Lett.*, *284*, 219–227, doi:10.1016/j.epsl.2009.04.031.

Courtier, A. M., et al. (2007), Correlation of seismic and petrologic thermometers suggests deep thermal anomalies beneath hotspots, *Earth Planet. Sci. Lett.*, *264*, 308–316, doi:10.1016/j.epsl.2007.10.003.

Courtillot, V., A. Davaille, J. Besse, and J. Stock (2003), Three distinct types of hotspots in the Earth's mantle, *Earth Planet. Sci. Lett.*, *205*, 295–308, doi:10.1016/S0012-821X(02)01048-8.

Davies, G. (1988), Ocean bathymetry and mantle convection: 1. Large-scale flow and hotspots, *J. Geophys. Res.*, *93*, 10,467–10,480, doi:10.1029/JB093iB09p10467.

Dziewonski, A. M., and D. L. Anderson (1981), Preliminary reference Earth model, *Phys. Earth Planet. Inter.*, *25*, 297–356, doi:10.1016/0031-9201(81)90046-7.

Escrig, S., P. Schiano, J.-G. Schilling, and C. Allègre (2005), Rhenium–osmium isotope systematics in MORB from the Southern Mid-Atlantic Ridge (40°–50°S), *Earth Planet. Sci. Lett.*, *235*, 528–548, doi:10.1016/j.epsl.2005.04.035.

Gibson, S., R. Thompson, J. Day, S. Humphris, and A. Dickin (2005), Melt-generation processes associated with the Tristan mantle plume: Constraints on the origin of EM-1, *Earth Planet. Sci. Lett.*, *237*, 744–767, doi:10.1016/j.epsl.2005.06.015.

Hanan, B., and D. Graham (1996), Lead and helium isotope evidence from oceanic basalts for a common deep source of mantle plumes, *Science*, *272*, 991–995, doi:10.1126/science.272.5264.991.

Hanan, B. B., J. Blichert-Toft, D. G. Pyle, and D. M. Christie (2004), Contrasting origins of the upper mantle revealed by hafnium and lead isotopes from the Southeast Indian Ridge, *Nature*, *432*, 91–94, doi:10.1038/nature03026.

Hart, S. R. (1984), A large-scale isotope anomaly in the Southern Hemisphere mantle, *Nature*, *309*, 753–757, doi:10.1038/309753a0.

Hart, S. R. (2011), The Mantle Zoo: New species, endangered species, extinct species, *Mineral. Mag.*, *3*, 983.

Hart, S. R., E. Hauri, L. Oschmann, and J. Whitehead (1992), Mantle plumes and entrainment: Isotopic evidence, *Science*, *256*, 517–520, doi:10.1126/science.256.5056.517.

Hawkesworth, C. J., M. S. M. Mantovani, P. N. Taylor, and Z. Palacz (1986), Evidence from the Parana of south Brazil for a continental contribution to Dupal basalts, *Nature*, *322*, 356–359, doi:10.1038/322356a0.

Hofmann, A. (2003), Sampling mantle heterogeneity through oceanic basalts: Isotopes and trace elements, in *Treatise on Geochemistry*, vol. 2, *The Mantle and Core*, edited by R. W. Carlson, chap. 2, pp. 1–44, Elsevier, Amsterdam.

Iwamori, H., and F. Albarède (2008), Decoupled isotopic record of ridge and subduction zone processes in oceanic basalts by independent component analysis, *Geochem. Geophys. Geosyst.*, *9*, Q04033, doi:10.1029/2007GC001753.

Kellogg, L. H., B. H. Hager, and R. D. van der Hilst (1999), Compositional stratification in the deep mantle, *Science*, *283*, 1881–1884, doi:10.1126/science.283.5409.1881.

Konter, J. G., B. B. Hanan, J. Blichert-Toft, A. A. P. Koppers, T. Plank, and H. Staudigel (2008), One hundred million years of mantle geochemical history suggest the retiring of mantle plumes is premature, *Earth Planet. Sci. Lett.*, *275*, 285–295, doi:10.1016/j.epsl.2008.08.023.

Labrosse, S., J. W. Hernlund, and N. Coltice (2007), A crystallizing dense magma ocean at the base of Earth's mantle, *Nature*, *450*, 866–869, doi:10.1038/nature06355.

Lee, C.-T., P. Luffi, T. Plank, H. Dalton, and W. Leeman (2009), Constraints on the depths and temperatures of basaltic magma generation on Earth and other terrestrial planets using new thermobarometers for mafic magmas, *Earth Planet. Sci. Lett.*, *279*, 20–33, doi:10.1016/j.epsl.2008.12.020.

McNamara, A. K., and S. Zhong (2005), Thermochemical structures beneath Africa and the Pacific Ocean, *Nature*, *437*, 1136–1139, doi:10.1038/nature04066.

Milner, S. C., and A. P. le Roex (1996), Isotope characteristics of the Okenyenya igneous complex, northwestern Namibia: Constraints on the composition of the early Tristan plume and the origin of the EM 1 mantle component, *Earth Planet. Sci. Lett.*, *141*, 277–291, doi:10.1016/0012-821X(96)00074-X.

Montelli, R., G. Nolet, F. Dahlen, and G. Masters (2006), A catalogue of deep mantle plumes: New results from finite-frequency tomography, *Geochem. Geophys. Geosyst.*, *7*, Q11007, doi:10.1029/2006GC001248.

Peate, D. W., C. J. Hawkesworth, M. S. M. Mantovani, N. W. Rogers, and S. P. Turner (1999), Petrogenesis and stratigraphy of the high-Ti/Y Urubici magma type in the Parana Flood Basalt Province and implications for the nature of the 'Dupal'-type mantle in the South Atlantic region, *J. Petrol.*, *40*, 451–473, doi:10.1093/petrology/40.3.451.

Ray, T. W., and D. L. Anderson (1994), Spherical disharmonics in the Earth sciences and the spatial solution: Ridges, hotspots, slabs, geochemistry and tomography correlations, *J. Geophys. Res.*, *99*, 9605–9614, doi:10.1029/94JB00340.

Regelous, M., Y. Niu, W. Abouchami, and P. Castillo (2009), Shallow origin for South Atlantic Dupal Anomaly from lower continental crust: Geochemical evidence from the Mid-Atlantic Ridge at 26°S, *Lithos*, *112*, 57–72, doi:10.1016/j.lithos.2008.10.012.

Salters, V. J. M., and A. Sachi-Kocher (2010), An ancient metasomatic source for the Walvis Ridge basalts, *Chem. Geol.*, *273*, 151–167, doi:10.1016/j.chemgeo.2010.02.010.

Schubert, G., G. Masters, P. Olson, and P. Tackley (2004), Superplumes or plume clusters?, *Phys. Earth Planet. Inter.*, *146*, 147–162, doi:10.1016/j.pepi.2003.09.025.

Simmons, N. A., A. M. Forte, and S. P. Grand (2007), Thermochemical structure and dynamics of the African superplume, *Geophys. Res. Lett.*, *34*, L02301, doi:10.1029/2006GL028009.

Sleep, N. (1990), Hotspots and mantle plumes: Some phenomenology, *J. Geophys. Res.*, *95*, 6715–6736, doi:10.1029/JB095iB05p06715.

Steinberger, B. (2000), Plumes in a convecting mantle: Models and observations for individual hotspots, *J. Geophys. Res.*, *105*, 11,127–11,152, doi:10.1029/1999JB900398.

Steinberger, B., and M. Antretter (2006), Conduit diameter and buoyant rising speed of mantle plumes: Implications for the motion of hot spots and shape of plume conduits, *Geochem. Geophys. Geosyst.*, *7*, Q11018, doi:10.1029/2006GC001409.

Thorne, M. S., E. J. Garnero, and S. P. Grand (2004), Geographic correlation between hot spots and deep mantle lateral shear-wave velocity gradients, *Phys. Earth Planet. Inter.*, *146*, 47–63, doi:10.1016/j.pepi.2003.09.026.

Torsvik, T. H., M. A. Smethurst, K. Burke, and B. Steinberger (2006), Large igneous provinces generated from the margins of the large low-velocity provinces in the deep mantle, *Geophys. J. Int.*, *167*, 1447–1460.

Torsvik, T. H., B. Steinberger, R. M. Cocks, and K. Burke (2008), Longitude: Linking Earth's ancient surface to its deep interior, *Earth Planet. Sci. Lett.*, *276*, 273–282, doi:10.1016/j.epsl.2008.09.026.

Wen, L., and D. L. Anderson (1997), Slabs, hotspots, cratons and mantle convection revealed from residual seismic tomography in the upper mantle, *Phys. Earth Planet. Inter.*, *99*, 131–143, doi:10.1016/S0031-9201(96)03162-7.

Wessel, P., and W. H. F. Smith (1991), Free software helps map and display data, *Eos Trans. AGU*, *72*(41), 441, doi:10.1029/90EO00319.

Wolfe, C. J., S. C. Solomon, G. Laske, J. A. Collins, R. S. Detrick, J. A. Orcutt, D. Bercovici, and E. H. Hauri (2009), Mantle shear-wave velocity structure beneath the Hawaiian hot spot, *Science*, *326*, 1388–1390, doi:10.1126/science.1180165.

Zindler, A., and S. R. Hart (1986), Chemical geodynamics, *Annu. Rev. Earth Planet. Sci.*, *14*, 493–571, doi:10.1146/annurev.ea.14.050186.002425.